Pressure-induced structural transformations in pure and Ru-doped $0.9PbZn_{1/3}Nb_{2/3}O_3$-$0.1PbTiO_3$ near the morphotropic phase boundary

N. Waeselmann,[1,*] B. J. Maier,[1] B. Mihailova,[1,†] R. J. Angel,[1,2,3] J. Zhao,[2] M. Gospodinov,[3,4] C. Paulmann,[1] N. Ross,[2] and U. Bismayer[1]

[1]*Department Geowissenschaften, Universität Hamburg, Grindelallee 48, 20146 Hamburg, Germany*
[2]*Virginia Tech Crystallography Laboratory, Department of Geosciences, Virginia Tech, Blacksburg, Virginia 24060, USA*
[3]*Dipartimento di Geoscienze, Universita degli studi di Padova, via G. Gradenigo 6, 35131 Padova, Italy*
[4]*Institute of Solid State Physics, Bulgarian Academy of Sciences, Boulevard Tzarigradsko Chausse 72, 1784 Sofia, Bulgaria*

Pressure-induced structural transformations in relaxor-based perovskite-type (ABO$_3$) $0.9PbZn_{1/3}Nb_{2/3}O_3$-$0.1PbTiO_3$ single crystals which have a very high piezoelectric response were studied by single-crystal x-ray diffraction and Raman spectroscopy at room temperature and pressures up to 18.1 GPa. Changes in the state of long-range order were observed near 1.0, 2.1, and 5.9 GPa. Initially, upon pressure increase, the ferroic deviation of the atomic positions from the cubic structure is reduced, but the ferroelectric twinning is enhanced, and near 1.0 GPa, the intrinsic ferroelectric multiphase domain pattern formed in the as-synthesized crystals is changed. At 2.1 GPa, the system undergoes a phase transition from a ferroelectric to a relaxor state, which exhibits an average cubic structure but still contains polar nanoregions. At 5.9 GPa, a reversible phase transition typical of Pb-based perovskite-type relaxors occurs, namely a cubic-to-antiferrodistortive phase transition resulting in a long-range order of antiphase octahedral tilts. On decompression, the ferroelectric state reappears below 2.1 GPa, and the local atomic structure is fully recovered at ambient pressure, but the final domain texture differs from the initial one. Ruthenium doping on the B site does not influence the pressure-induced structural transformations.

I. INTRODUCTION

Lead-based relaxor ferroelectrics with the perovskite-type structure (ABO$_3$) show a broad and frequency-dispersive maximum of the dielectric permittivity. These materials have been extensively studied over the last decade due to their superb dielectric, electro-elastic, and electro-optical properties.[1] Particular interest has been directed towards solid solutions between relaxor and normal ferroelectrics, such as $(1-x)PbZn_{1/3}Nb_{2/3}O_3$-$xPbTiO_3$ (PZN-xPT) and $(1-x)PbMg_{1/3}Nb_{2/3}O_3$-$xPbTiO_3$ (PMN-xPT), which show an extremely high piezoelectric response close to the morphotropic phase boundary (MPB).[2,3] For PZN-xPT, the MPB corresponds to $x \sim 0.08$–0.10.[4] For x values smaller than 0.08, the symmetry of the ferroelectric phase is rhombohedral, whereas compounds with $x > 0.10$ exhibit tetragonal symmetry below the para-to-ferroelectric phase-transition temperature. The room-temperature structure of PZN-xPT on the MPB is still a matter of controversy and it has been proposed that it is of monoclinic[5] or orthorhombic symmetry[4] or a coexistence of tetragonal and nontetragonal ferroelectric long-range order.[6,7] Similar to other perovskite-type (ABO$_3$) relaxors, at temperatures higher than the dielectric-permittivity maximum T_m, PZN-xPT undergoes two nanoscale structural transformations on cooling:[8–12] a nucleation of dynamic polar clusters at the Burns temperature $T_B \sim 730$ K via coupling of incoherent atomic displacements from their positions in the ideal perovskite structure and, at the intermediate temperature $T^* \sim 525$ K, merging of the already-formed polar clusters into larger polar nanoregions, which results in slower flipping dynamics. On further cooling, PZN-xPT crystals with x values near the MPB undergo two phase transitions:[4,5,10] cubic to polar tetragonal at $T_{C1} \sim 450$ K and polar tetragonal to polar

monoclinic (or orthorhombic) at $T_{C2} \sim 340$ K. However, the development of ferroelectric long-range order is incomplete, and even below T_{C2}, a fraction of polar nanoregions still persist.[12,13] The high structural complexity on the mesoscopic scale makes it difficult to understand the structure-property relations in PZN-xPT and PMN-xPT and, in particular, to clarify whether the high piezoelectric effect is mainly due to the coexistence of two ferroelectric phases or due to the multiple domain walls associated with monoclinic domains or due to the coexistence of polar nanoregions with long-range-ordered ferroelectric domains.

Studying the response of the structure to external pressure can help in the understanding of the structural peculiarities of relaxor-based piezoelectrics. Dielectric experiments at low pressures (below 1.5 GPa) showed that pressure enhances the relaxor behavior in relaxor-based piezoelectrics,[14,15] but the pressure-induced relaxor state is different from the low-temperature nonergodic relaxor state, which consists of frozen polar nanoregions.[15] Also, it has been demonstrated that the application of low pressures (below 1 GPa) on [001]-poled $PbB'_{1/3}B''_{2/3}O_3$-xPT of a composition that is near the MPB considerably decreases the transverse piezoelectric and electromechanical response but only slightly lowers the corresponding longitudinal responses.[16,17] High-pressure structural studies of solid solutions between relaxors and normal ferroelectrics are, however, rare,[18,19] and in particular, the high-pressure structure of PZN-xPT at the MPB has not been analyzed yet. *In-situ* high-pressure diffraction and Raman scattering analysis of relaxors of the type $PbB'_{1/3}B''_{2/3}O_3$[20–22] and $PbB'_{1/2}B''_{1/2}O_3$[23–25] revealed that pressure suppresses the mesoscopic polar order (i.e. reduces the length of coherence of polar cation shifts), which facilitates the occurrence of at least two pressure-induced phase transitions below 30 GPa. The first

pressure-induced phase transition involves the development of long-range antiphase octahedral tilt order, while the second one consists of a symmetry reduction of the tilt configuration and may also involve the development of long-range order of antiferroelectric off-centered displacements of the Pb cations.[25] The pressure dependence of the Raman scattering for relaxor-based piezoelectric solid solutions[18,19] suggests that pressures up to 10 GPa induce structural transformations similar to those observed in pure relaxor compounds.

The objective of this study was to elucidate the pressure-induced structural phenomena in relaxor-based piezoelectrics close to the MPB on the basis of combined *in-situ* single-crystal x-ray diffraction and Raman spectroscopy of PZN-0.1PT in the pressure range up to 18.1 GPa. In addition, Ru-doped PZN-0.1PT has been studied by high-pressure Raman spectroscopy, as it has been recently shown that a small amount of ruthenium significantly hardens the hysteresis loops of polarization- and strain-electric field[7] and extends the temperature range in which the tetragonal structure is preferred.[12]

II. EXPERIMENTAL DETAILS

Optically and chemically homogenous single crystals of PZN-0.1PT and PZN-0.1PT:Ru with the ratio Ru/Ti ∼ 0.02 were synthesized by the high-temperature solution growth method.[7] The chemical compositions of the as-grown single crystals were determined by electron microprobe analysis (Cameca Microbeam SX100) averaging over 50 points from each specimen. The relative error in the x value was 0.3% as determined from the standard deviation of Ti content, whereas the standard deviation of the Ru content was ∼35%. The Ru doping changed the appearance of PZN-0.1PT from transparent and yellow in color to opaque with a metallic luster.

The *in-situ* high-pressure x-ray diffraction (XRD) and Raman spectroscopic experiments were conducted in diamond anvil cells (DACs). Stainless steel gaskets and 4:1 methanol-ethanol or 16:3:1 methanol-ethanol-water mixtures as pressure-transmitting media were used for the experiments up to 9.8 GPa, which is the hydrostatic limit of these alcohol mixtures.[26] To obtain hydrostatic conditions above 9.8 GPa and better stability of the sample chamber formed by the drilled gasket, He was used as a pressure medium, and rhenium was used for the gasket. The measurements were conducted on plates oriented parallel to the cubic {100} planes. The size of the samples measured in alcohol mixtures from ambient pressure up to 9.8 GPa was approximately 135 × 100 × 40 μm, whereas that of the sample measured in He between 6.9 and 18.1 GPa was 70 × 50 × 30 μm. Three different designs of DACs were used in the experiments. For Raman spectroscopy up to 9.8 GPa, a gas-membrane-driven easyLab Diacell μScopeDAC-RT(G) was used. For single-crystal synchrotron XRD as well as Raman spectroscopy between 6.9 and 18.1 GPa, DACs of the Boehler–Almax design[27] were used. For in-house single-crystal diffraction measurements, an ETH DAC[28] was used. The pressure values in the synchrotron XRD and Raman scattering experiments were determined by the ruby-fluorescence method with an accuracy of 0.1 GPa.[29]

The pressure dependence of the pseudocubic unit-cell parameters was measured with a Huber four-circle single-crystal diffractometer, using the method of eight-position

diffraction beam centering, which ensures a precision in the relative volume $V(p)/V_0 \sim 0.0001$.[30] In these experiments, the pressure values were determined with a precision of 0.01 GPa from the measured volume and the previously determined equation of state of a quartz crystal loaded next to the sample.[31]

Synchrotron single-crystal XRD was performed at the F1 beamline at HASYLAB/DESY using a MarCCD 165 detector. Data were collected with a radiation wavelength of $\lambda = 0.5000$ Å, a sample-to-detector distance of 100 mm, a step width of $0.5°$ per frame, 80 frames per measurement, and an exposure time of 120 s per frame. Reciprocal-space sections were reconstructed from the raw data frames using the CRYSALIS Oxford Diffraction software.

Unpolarized Raman spectra were collected using a Horiba Jobin–Yvon T64000 triple-grating spectrometer equipped with an Olympus BH41 microscope and a 50× long-working-distance objective. The measurements were conducted in a backscattering geometry using the 514.5-nm line of an Ar$^+$ laser and a spectral resolution of 2 cm^{-1}. The laser power surface density delivered to the DAC was 1.6 kW/mm^2. Pure PZN-0.1PT was measured with an acquisition time of 15 or 20 s, whereas the acquisition time for the Ru-doped compound was 30 s. The as-measured spectra were reduced by the Bose–Einstein phonon occupation factor to eliminate the effect of temperature on the peak intensities and were fitted with Lorentzian functions to determine the peak positions, full widths at half maximum (FWHMs), and integrated intensities, using the software package Origin 8.5.

III. RESULTS AND DISCUSSION

At ambient pressure and room temperature, coexisting tetragonal and nontetragonal ferroelectric domains have been detected by piezoresponse force microscopy[7] performed on pure and Ru-doped PZN-0.1PT crystals from the same synthesis batches as the crystals studied here. Further, the majority of diffraction studies of PZN-xPT at the MPB indicate that the monoclinic domains are dominant at ambient conditions.[5,32] Our polarized Raman scattering analysis on PZN-0.1PT also suggests an abundance of monoclinic domains at ambient conditions.[12] Therefore, a structure in which different types of ferroelectric domains, but with a predominance of monoclinic domains, was the starting point in the interpretation of the new high-pressure data presented here.

A. XRD analysis of PZN-0.1 PT

The FWHM of representative Bragg peaks recorded in high-precision in-house single-crystal XRD experiments as well as the unit-cell parameters and interaxial angles obtained from symmetry-unconstrained unit-cell refinements to the diffracted beam positions are shown in Fig. 1. Due to the small structural deviation of the ferroelectric phases from the cubic phase, an apparent splitting of the cubic Bragg peaks was not resolved at ambient pressure, only a slight broadening of these peaks. Note that in single-crystal XRD experiments on pseudocubic multidomain samples, a broadening of the diffraction peaks plotted against the 2θ angle (d spacing) results from the ferroic distortion of the atomic structure, while a peak broadening vs the angle of rotation about the
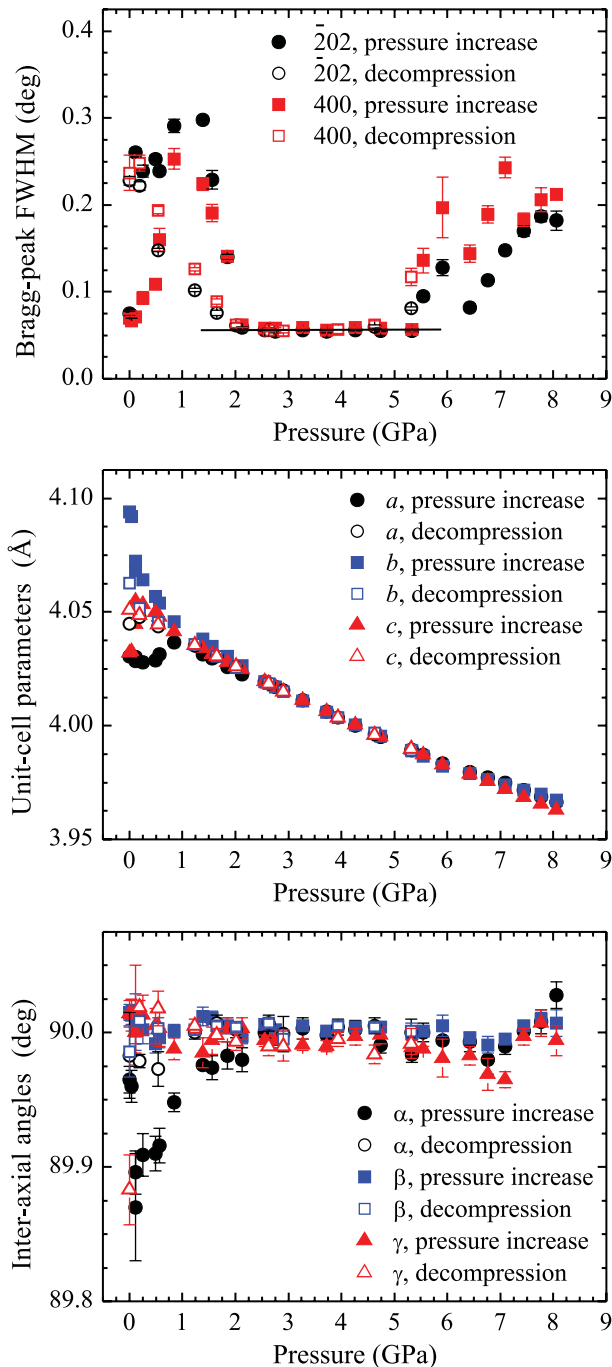
FIG. 1. (Color online) Pressure dependence of the FWHM of two representative Bragg peaks (Miller indices refer to $Fm\bar{3}m$) (upper plot), unit-cell parameters (middle plot), and angles (bottom plot) obtained from symmetry-unconstrained unit-cell refinements to single-crystal XRD data. The filled and open symbols correspond to data collected on pressure increase and on decompression, respectively. The error bars for the unit-cell parameters are within the size of the symbols. The horizontal line in the upper plot marks the instrumental resolution.

perpendicular axis (rocking curves) results from the mutual misorientation of the domains.[33] In Fig. 1, we show the FWHMs from the rocking curves of the corresponding Bragg reflections, and therefore, the pressure dependences of these

FWHMs represent purely the pressure-induced change in the degree of domain misorientation. At the same time, the deviation of unit-cell parameters from cubic is sensitive to the overall ferroic distortion of the atomic structure, regardless of the degree of ferroic twinning. For PZN-0.1PT, the measured unit-cell parameters at ambient conditions correspond to a monoclinic metric, but this fact does not mean that other types of ferroic domains are absent from the structure. The pressure dependences of the Bragg-peak widths and the unit-cell parameters (Fig. 1) reveal four distinguishable ranges of pressure-induced structural states. Between ambient pressure and 1.0 GPa, the ferroelectric distortion of the atomic structure is reduced because the unit-cell parameters evolve towards cubic, but the distribution of domain orientations is enhanced, as seen from the strong broadening of the diffraction peaks. This is not the usual pattern of behavior for a ferroic multidomain sample in which one would expect a decrease in the mutual misorientation between domains when the ferroic distortion of the atomic structure is reduced. Hence, the pressure evolution of both the unit-cell parameters and FWHMs indicates an enhancement of the ferroic twinning (more and smaller domains with smaller ferroic distortion) in the pressure range up to 1 GPa. We suggest that this process occurs due to the competitive coexistence of different types of ferroelectric domains as one of these phases is being suppressed as pressure increases to 1.0 GPa. This is consistent with the abrupt change in the pressure dependencies of the diffraction-peak widths and unit-cell parameters at 1 GPa. On further pressure increase up to 2.1 GPa, the peak broadening strongly decreases and the deviation of the unit-cell parameters from cubic decreases, consistent with the evolution of a ferroic single-phase multidomain sample towards cubic symmetry. Between 2.1 and 5.2 GPa, neither broadening of the diffraction peaks nor deviation of the unit-cell parameters from cubic were detected, indicating that the average structure is cubic. Above 5.2 GPa, the Bragg peaks again start broadening with pressure increase, and the unit-cell parameters slightly deviate from cubic, which indicates the development of a new ferroic state. The dependence of the normalized pressure $F = p/[3f(1 + 2f)^{5/2}]$ on the Eulerian strain $f = [(V_0 - V)^{2/3} - 1]/2$ calculated from the measured dependence of the unit-cell volume V on the pressure p (see Fig. 2) also indicates the existence of three pressure-induced structural transformations near 1.0, 2.1, and 5.9 GPa.

To shed light on the structural state above 2.1 GPa, we have conducted synchrotron single-crystal XRD. Figure 3 shows representative sections of $(hk0)$ and $(hk1)$ reciprocal-space layers of PZN-0.1PT under pressure. The Miller indices throughout the whole paper are given with respect to $Fm\bar{3}m$, which is the symmetry of the cubic double-perovskite structure. It is well known that polar nanoregions in Pb-based relaxors give rise to diffuse scattering streaks along the cubic reciprocal-space $\langle 110\rangle^*$ directions.[13,34,35] Weak x-ray diffuse scattering along $\langle 110\rangle^*$ can be seen up to 4.0 GPa, revealing the existence of polar nanoregions. Therefore, at 2.1 GPa, PZN-0.1PT reaches a relaxor cubic state with no ferroelectric long-range order, which is consistent with dielectric experiments indicating a ferroelectric-relaxor crossover at moderate pressures.[14,15] X-ray diffuse streaks were not observed at 5.0 GPa and above, indicating that
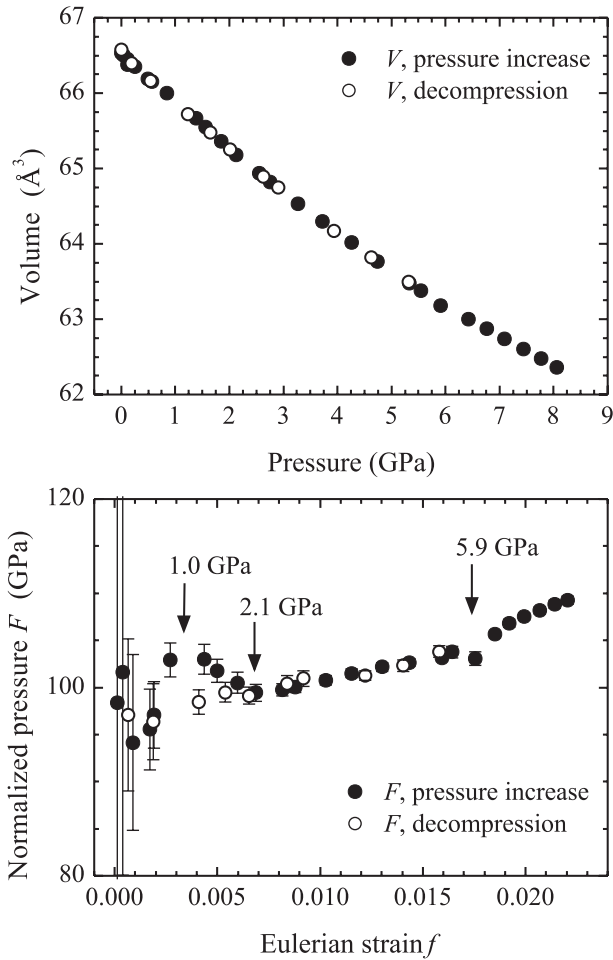
FIG. 2. Unit-cell volume V vs pressure p measured in high-precision single-crystal XRD experiments (upper plot) and the corresponding $F(f)$ dependence (bottom plot), where F is the normalized pressure $F = p/[3f(1 + 2f)^{5/2}]$ and f is the Eulerian strain $f = [(V_0 - V)^{2/3} - 1]/2$. The filled and open symbols correspond to data collected on pressure increase and on decompression, respectively. The error bars for the unit-cell volume are within the size of the symbols.

the relaxor state of PZN-0.1PT persists up to 4 GPa, but at 5 GPa, the polar order is destroyed even on the mesoscopic scale. At 5.9 GPa, a new class of sharp Bragg peaks with h, k, l, all odd, appear (see Fig. 3). Previously, we have shown for other Pb-based perovskite-type relaxors[24,36–38] that such pressure-induced Bragg reflections are associated with the development of antiphase octahedral tilts of type $a^- a^- a^-$ (Glazer's notation[39]) and a consequent change of the symmetry from primitive cubic $Pm\bar{3}m$ to rhombohedral $R\bar{3}c$, in the case of absence of long-range chemical B-site order of NaCl type, or from face-centered cubic $Fm\bar{3}m$ to rhombohedral $R\bar{3}$, if a long-range chemical B-site order is presented. At ambient pressure, PZN-0.1PT does not exhibit any superlattice Bragg peaks indicative of long-range chemical B-site order.[12] Hence, the synchrotron XRD data in PZN-0.1PT clearly reveal the occurrence of a continuous phase transition from primitive cubic to rhombohedral $R\bar{3}c$ symmetry comprising a long-range order of antiphase tilts of equal magnitude typical of Pb-based perovskite-type relaxors.[20,22,40] No other pressure-induced Bragg peaks or d-space splitting of the existing diffraction
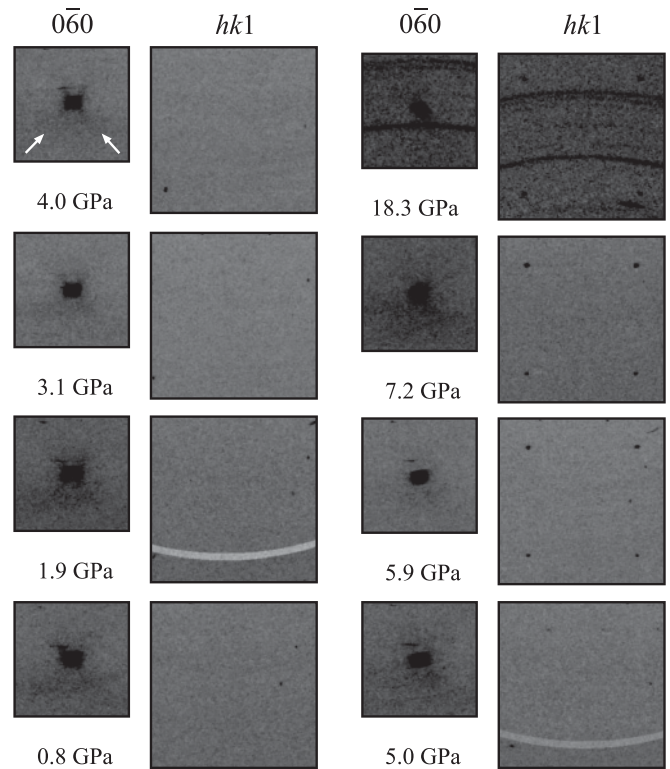

FIG. 3. Reciprocal-space layers reconstructed from synchrotron single-crystal XRD on PZN-0.1PT. The Miller indices refer to a cubic double-perovskite $Fm\bar{3}m$ unit cell. The arrows in the sector around the $0\bar{6}0$ Bragg peak mark the diffuse scattering along $\langle 110 \rangle^*$. The sectors of $(hk1)$ layers demonstrate that pressure-induced odd-odd-odd Bragg peaks appear at 5.9 GPa; the reflections in the upper-left and bottom-right corner are $\bar{1}\bar{3}1$ and $1\bar{5}1$, respectively.

peaks were detected up to 18.1 GPa, indicating that no further phase transitions occur in this pressure range. Figure 4 depicts the pressure dependences of the integrated intensities of representative Bragg peaks with $h + k + l = 4n + 2$ and h, k, l all equal to $2n + 1$ calculated from the synchrotron XRD data. The third class of observed Bragg peaks, having $h + k + l = 4n$, was oversaturated in the whole pressure range. As can be seen in Fig. 4, the intensities of the pressure-induced odd-odd-odd peaks generated from antiphase octahedral tilts increase from 5.9 to $\sim$11 GPa and then become saturated. The intensities of the peaks with $h + k + l = 4n + 2$ initially decrease with the pressure increase, then remain nearly constant in the range 3–5 GPa, and above 5.9 GPa, show the same trend as the odd-odd-odd Bragg peaks. All atoms of the perovskite structure contribute to the Bragg peaks with $h + k + l = 4n + 2$, with the more heavily-scattering A- and B-site cations contributing to the scattering factor with opposite signs. Thus, the pressure evolution of the intensities of these peaks reflects the suppression of long-range polar order of the cations at moderate pressures and the subsequent development of antiferrodistortive order of the oxygen atoms above 5.9 GPa. The saturation in the intensities above 11 GPa indicates that the fraction of ferroic domains with long-range octahedral tilting as well as the octahedral tilt angle then becomes essentially constant at higher pressures.
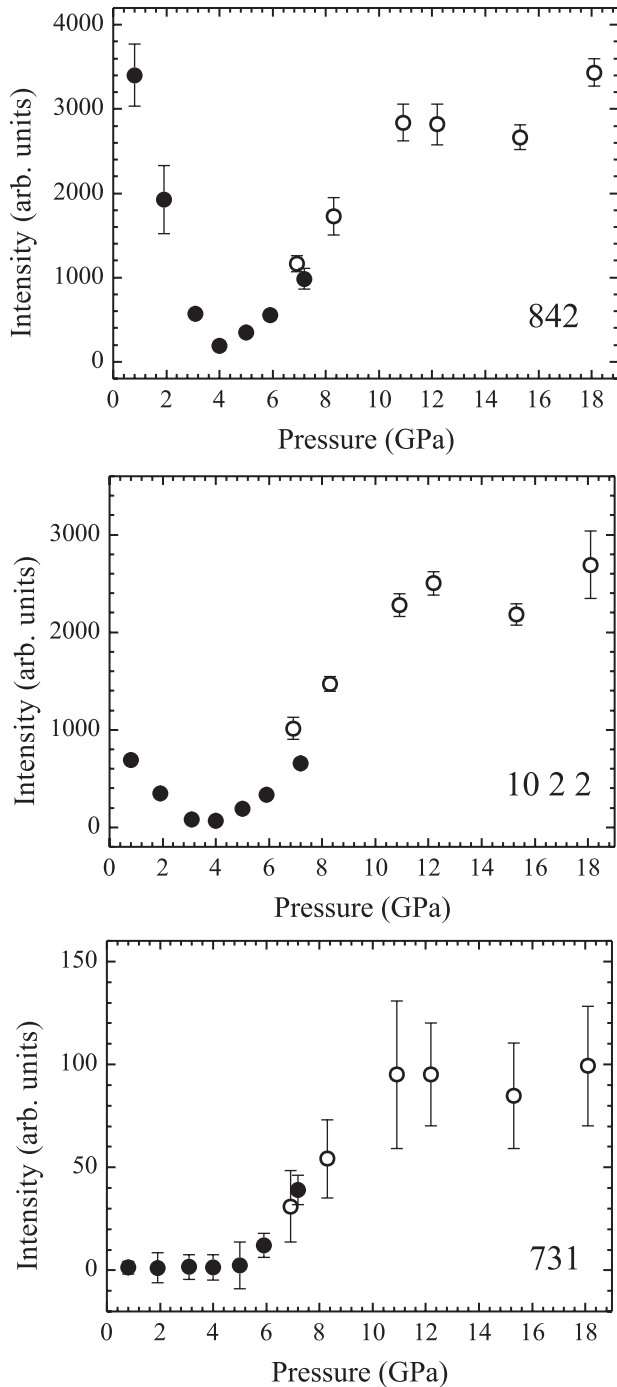
FIG. 4. Integrated intensities of Bragg peaks measured in single-crystal synchrotron experiments. The intensities are averaged over the peaks which are symmetry-equivalent in the prototype cubic structure. The filled and open symbols correspond to measurements in methanol-ethanol and in He as pressure-transmitting media, respectively; the intensities were normalized to volume of the corresponding sample. Miller indices refer to $Fm\bar{3}m$.

B. Raman scattering of PZN-0.1PT

Raman spectra of PZN-0.1PT collected at different pressures up to 18.1 GPa are shown in Fig. 5. As for all Pb-based relaxor ferroelectrics, the Raman scattering of PZN-0.1PT can be understood only in terms of a double-perovskite
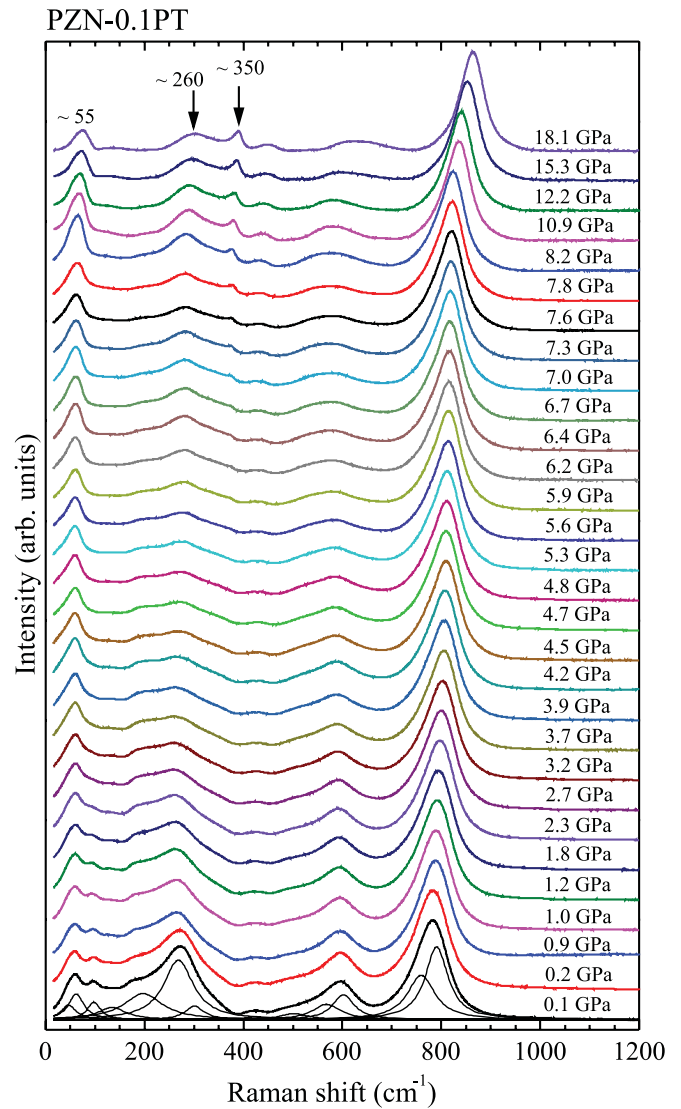

FIG. 5. (Color online) Raman spectra of PZN-0.1PT measured up to 18.1 GPa.

structure, regardless of the presence or absence of long-range chemical B-site disorder.[12,40–43] The Γ-point optical modes of the prototype cubic structure $Fm\bar{3}m$ are $A_{1g}(R) + E_g(R) + F_{2u}(ina) + 2F_{2g}(R) + 4F_{1u}(IR) + F_{1g}(ina)$, where R, IR, and ina stand for Raman-active, infrared-active, and inactive, respectively.[44] We have analyzed in detail the Raman scattering near 55, 260, and 350 cm^{-1}, which has been proven to be highly sensitive to pressure-induced structural transformations in other Pb-based relaxor materials.[19,21–25,38,42,45]

The band near 55 cm^{-1} originates from Pb-localized modes related to a Raman-active F_{2g} mode of the prototype structure. For compounds of the type $PbB'_{1/3}B''_{2/3}O_3$-xPT with x varying between zero and the value corresponding to the MPB, this band is a doublet at high temperatures due to the existence of two cubic local states of the Pb ions having distinct local chemical environments formed by the nearest B-site cations.[12] However, at temperatures below the para-to-ferroelectric phase transition, the two Pb states related to the chemical environment become dynamically indistinguishable, and hence the doubling of the peak near 55 cm^{-1} results from the lowering
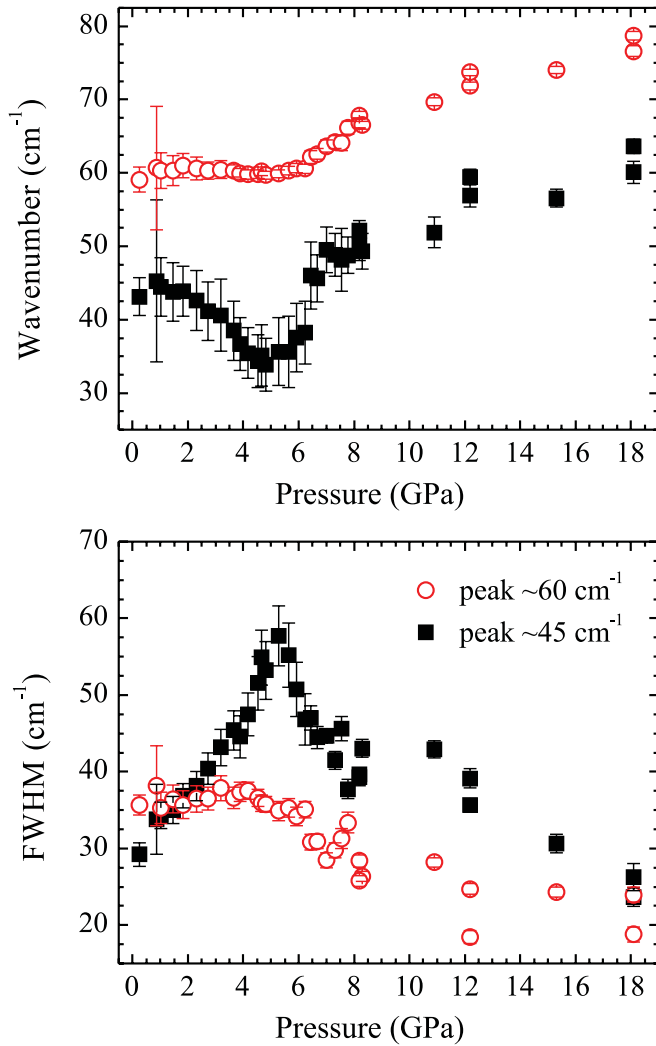
FIG. 6. (Color online) Pressure dependence of the wave number and FWHM of the two components of the Raman-scattering band near 55 cm^{-1} observed for PZN-0.1PT, which arises from Pb-localized modes.

of the symmetry of the average structure.[12] Our *in-situ* high-pressure experiments on PZN-0.1PT were conducted at room temperature, which is below T_{C2},[10,12] and therefore the lower wave number component at ~45 cm^{-1} reflects the presence of ferroelectric long-range order. This Raman signal considerably softens and broadens when pressure is increased from ambient to ~4.5 GPa (see Fig. 6) due to the pressure-induced suppression of the polar order. At the critical pressure $p_c = 5.9$ GPa of the cubic-to-rhombohedral phase transition, the lower wave number component of the band at 55 cm^{-1} starts hardening and narrowing (see Fig. 6), following the behavior of a soft mode. Indeed, for Pb-based relaxors, the occurrence of a pressure-induced cubic-to-rhombohedral phase transition is accompanied by the appearance of a soft mode.[23,24,42] Thus, the origin of the Raman scattering near 45 cm^{-1} above 5.9 GPa is different from that below 4.5 GPa, i.e. two different phonon modes generate the lowest wave number Raman signal at low pressures and at high pressures. While at low pressures, this Raman signal arises from the long-range ferroelectric order, above 5.9 GPa, it is associated

with the development of long-range antiferrodistortive order, namely antiphase octahedral tilting. Between 4.5 and 5.9 GPa, the lowest wave number Raman signal does not disappear (see Fig. 6), meaning that the corresponding vibrational modes are still underdamped. This indicates that order-disorder structural processes contribute considerably to the pressure-induced structural transformations in PZN-0.1PT,[46] which is most probably related to the complex chemistry on the B site.

The Raman scattering near 260 cm^{-1} arises from off-center-displaced B-site cations,[42,47] and at ambient pressure, it is sensitive to the development of polar order, in particular to the coupling processes at T^*, where large polar nanoregions with slower dynamics are formed.[12,42,48] Similar to other relaxor and relaxor-related materials,[18,19,21–23,40,45] pressure reduces the intensity of the Raman scattering at 260 cm^{-1} observed for PZN-0.1PT (see Fig. 5), indicating a reduction of the polar shifts of the B-site cations. However, the effect is less pronounced for $PbB'_{1/3}B''_{2/3}O_3$-type systems[18,19,21,22] as compared to $PbB'_{1/2}B''_{1/2}O_3$-type relaxors[23,35] and relaxor-related materials with homovalent ions on the B site,[21,45] and PZN-0.1PT shows the same trend. Aliovalent A-site doping of $PbB'_{1/2}B''_{1/2}O_3$ relaxors also results in the persistence of the Raman signal near 260 cm^{-1} under pressure.[38] These findings indicate that local electric fields associated with charge imbalance on the A or B site of the perovskite structure oppose the tendency of external pressure to move the off-centered B-site cations back to the corresponding octahedral centers. For PZN-0.1PT, the wave number of the 260-cm^{-1}-peak rapidly increases at 4.5 GPa, and the FWHM vs pressure shows a broad maximum in the range 4.5–8 GPa (see Fig. 7). Synchrotron XRD data indicates that the polar nanoregions vanish above 4.0 GPa (see Fig. 3). Therefore, the polar B-cation shifts existing above 4.0 GPa are uncorrelated even on the mesoscopic scale. However, their existence apparently opposes the formation of long-range antiferrodistortive octahedral-tilt order and enhances the order-disorder structural phenomena in the pressure-induced phase transition at 5.9 GPa.

The Raman peak at 350 cm^{-1} (see Fig. 5) is related to the silent F_{2u} mode of the prototype cubic structure and is generated by Pb-O bond stretching within the cubic {111} planes.[42,47] This type of vibration can also be considered as antiphase octahedral tilting[40,44,47] as it changes the Pb-O bond lengths, and hence the peak is enhanced with pressure due to the development of static long-range ordered tilts. This peak is resolved in the cross-polarized Raman spectra of PZN-0.1PT measured at ambient pressure in air, but in the unpolarized spectra collected in the DAC, it was resolved only above 1.8 GPa. The position of the peak near 350 cm^{-1} strongly increases between 4.5 and ~7.0 GPa, while the FWHM strongly decreases and becomes nearly constant above 7 GPa (see Fig. 8). Similar pressure dependence has been observed for PMN-xPT.[19] Also, similar to other $PbB'_{1/3}B''_{2/3}O_3$-based materials,[18,19,22] the peak at 350 cm^{-1} of PZN-0.1PT is less enhanced with pressure as compared to Pb-based perovskites with a B-site stoichiometry equal or approximately equal to 1:1.[23,35,45] This again indicates a competition between uncoupled B-site off-centered displacements and antiphase tilt order in the vicinity of the pressure-induced phase transition at 5.9 GPa. The nearly constant FWHM above 7 GPa and
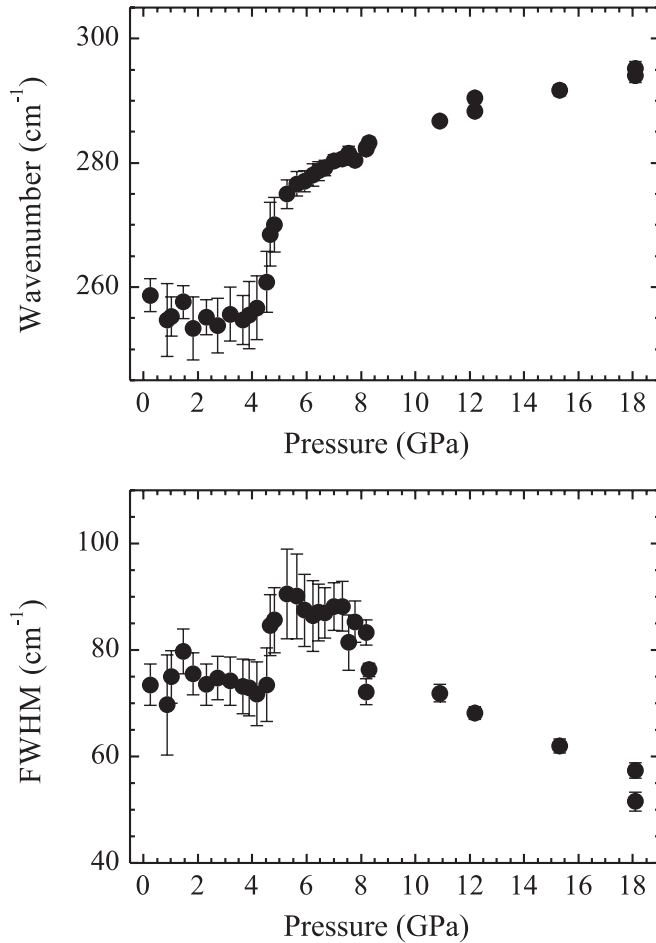
FIG. 7. Pressure dependence of the wave number and FWHM of the Raman peak near 260 cm^{-1} observed for PZN-0.1PT, which arises from vibrations of off-centered B-site cations.

FIG. 8. Pressure dependence of the wave number and FWHM of the Raman peak near 350 cm^{-1} observed for PZN-0.1PT, which arises from Pb-O bond stretching within cubic {111} planes and can be considered also as octahedral tilting.

the absence of any pressure-induced splitting of the peak at 350 cm^{-1}, as previously observed for other relaxors,[23,25] shows that, between 7 and 18.1 GPa, the oxygen environment of the Pb^{2+} cations remain the same even on the local scale.

It should be emphasized that according to Raman spectroscopy, after decompression, the atomic structure is fully recovered at ambient pressure. The increase in the FWHMs of the Bragg peaks (see Fig. 1) also indicates that the long-range ferroelectric order reappears below 2.1 GPa. However, the peak widths are different in detail from those measured prior to compression, and the deviation of the unit-cell parameters from cubic is considerably less than that of the initial structure. This indicates that the domain texture is different, and the overall ferroic distortion of the average structure is smaller as compared to the initial state. From this point of view, the phase transition at 1 GPa might be thought as being irreversible. However, the complete reversibility of the Raman scattering indicates that the predominant monoclinic atomic arrangements are recovered on decompression. Most probably, the correlation length of ferroic distortion in the final state is shorter than in the initial state, which results in smaller domains and a smaller deviation of the measured unit-cell parameters from the cubic values. It should be mentioned that, based only on the data presented here, one cannot state whether
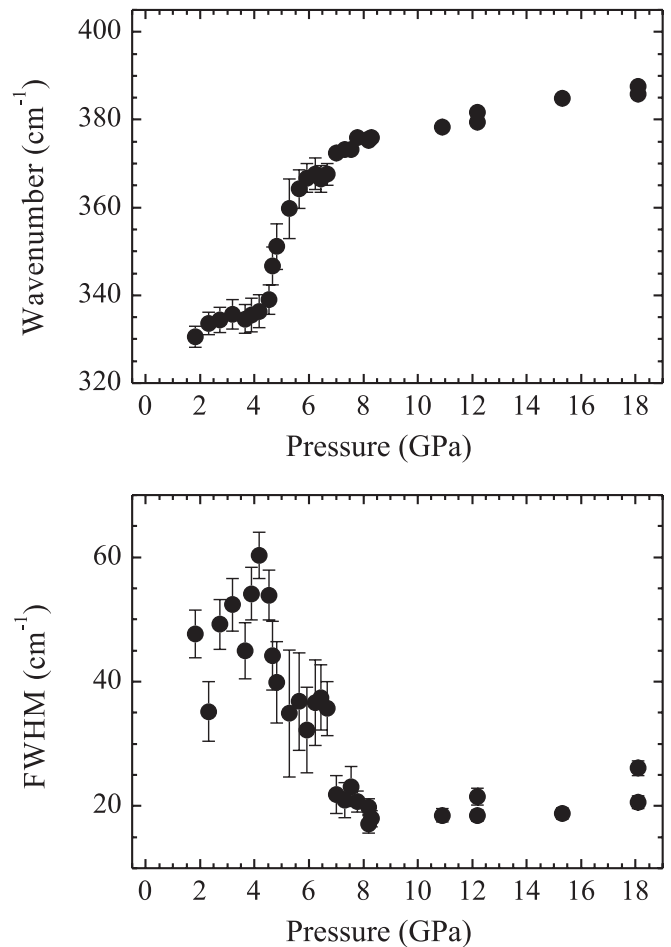
a second type of ferroelectric domains reappears or not on decompression.

C. Raman scattering of Ru-doped PZN-0.1PT

At ambient pressure, the addition even of a small amount of Ru [Ru/(Zn + Nb + Ti) ~ 0.002] leads to a substantial hardening of the polarization-field and strain-field hysteresis loops of PZN-0.1PT[7] and favors the tetragonal state in a wider temperature range compared to the undoped compound.[12] These effects are attributed to the fact that Ru substitutes for Ti, and at room temperature, the average valence of the ruthenium cations is between 4+ and 3+.[7] To check whether Ru doping influences the structural state at high pressures, we have conducted Raman scattering in the pressure range up to 8.4 GPa. According to the Raman spectra (see Fig. 9), Ru-doped PZN-0.1PT exhibits the same structural changes with pressure that have been observed for the pure compound (compare Figs. 5 and 9). The Raman scattering near 260 cm^{-1} is moderately suppressed with pressure increase, while that near 350 cm^{-1} is enhanced. The ratio between the integrated intensities of the peaks at 350 and 260 cm^{-1} (not shown) for pure and Ru-doped PZN-0.1PT is the same. This indicates
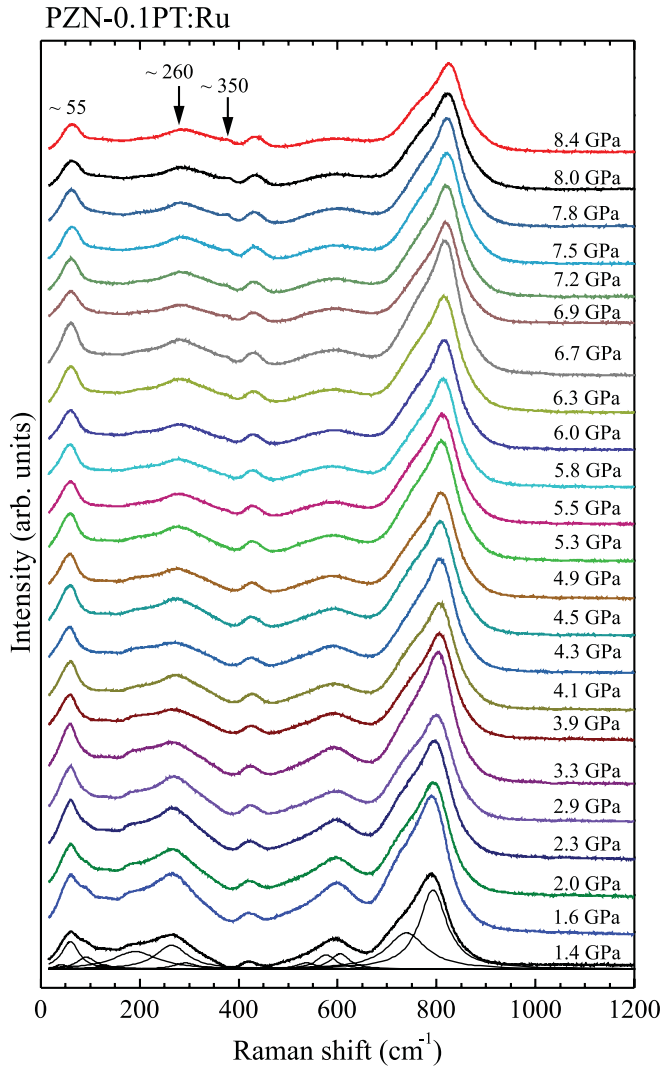
FIG. 9. (Color online) Raman spectra of Ru-doped PZN-0.1PT measured up to 8.4 GPa.
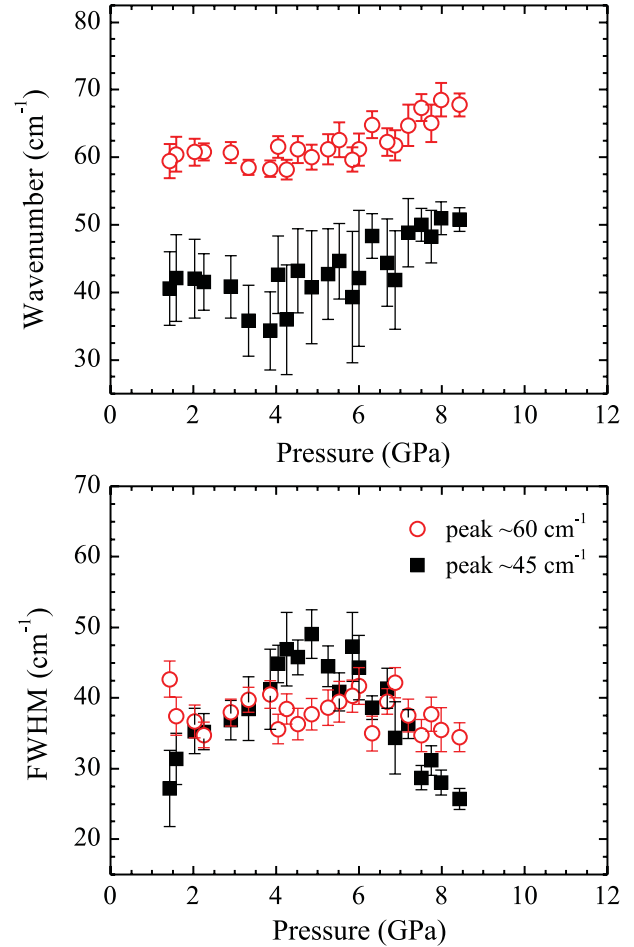

FIG. 10. (Color online) Pressure dependence of the wave number and FWHM of the two components of the Raman-scattering band near 55 cm^{-1} observed for Ru-doped PZN-0.1PT, which arises from Pb-localized modes. Note the difference between the X-axis scales in this figure and in Fig. 6.

that Ru doping does not influence the pressure-induced local structural changes, although at ambient pressure, Ru doping decreases the characteristic and critical temperatures.[12] Ru doping leads to overall broadening and larger overlaps of the Raman peaks, which results in larger uncertainties in the peak parameters derived from the fitting of the spectral profiles. The pressure dependencies of the two components of the band near 55 cm^{-1} for Ru-doped PZN-0.1PT are shown in Fig. 10. Similar to the pure compound, the FWHM of the peak near 45 cm^{-1} observed for Ru-doped PZN-0.1PT exhibits a maximum between 4.5 and 5.9 GPa. This peak also softens when pressure approaches 4.5 GPa and hardens at higher pressures, indicating the occurrence of the same cubic-to-rhombohedral phase transition as for pure PZN-0.1PT. Due to the large uncertainties, the exact value of the critical pressure cannot be determined from the pressure dependence of the position of the peak near 45 cm^{-1}. However, for both undoped and Ru-doped PZN-0.1PT the wave number of the peak near 60 cm^{-1} is constant until 5.9 GPa and then begins to harden. This indicates that Ru-doping does not change the critical

pressure, which is in accordance with the pressure dependence of the FWHM of the peak at 45 cm^{-1}.

D. Pressure- vs temperature-induced structural changes

Multistep structural transformations occur in PZN-01PT on both pressure increase and temperature decrease, and both thermodynamic parameters drive the system to a ferroic state. However, the high-pressure structural state significantly differs from the low-temperature structural state. At room temperature and pressures above 5.9 GPa, an antiferrodistortive long-range order is developed, and only uncoupled polar displacements of B-site cations exist. By contrast, at ambient pressure and temperatures below T_{C2}, two types of long-range polar order (ferroelectric domains), along with mesoscopic polar order (polar nanoregions), coexist, i.e. the structure is much more flexible and heterogeneous as compared to the high-pressure state. This most probably is the reason why low level of B-site doping with Ru influences the ferroelectric state below T_{C1}[12] but has a negligible effect on the pressure-induced cubic-to-antiferrodistortive phase transition.

Although there is a lack of high-pressure XRD studies on $PbMg_{1/3}Nb_{2/3}O_3$-xPbTiO$_3$ (PMN-xPT) close to the MPB, the similarities between PZN-0.1PT and PMT-xPT in the pressure evolution of the Raman scattering suggest that, upon pressure increase, PMN-xPT also reaches a cubic relaxor state and then develops antiferrodistortive order.

E. A note about the structure-property relation in $PbB'_{1/3}B''_{2/3}O_3$-PbTiO$_3$ binary systems

The origin of the giant piezolectric effect in ferroelectric solid solutions is still obscure.[49] In general, it can be related to the chemically induced complex domain structure in the vicinity of the MPB or to intrinsic structural inhomogeneities on the mesoscopic scale. The former case can be further subdivided into two cases: (i) coexistence of ferroelectric domains of different symmetry, i.e. competition between different types of long-range polar order, or (ii) existence of one type of low-symmetry domains, e.g. monoclinic or triclinic, which allows for a high density of domain walls. In both cases, the domain texture should play an important role for the giant response functions in this class of materials, and we should expect higher piezoelectric and electromechanical coefficients if the ferroelectric twinning is enhanced, i.e. the number of domains increases, and the mean domain size of the domains decreases. Our results indicate that, in the low-pressure range (from ambient pressure to 1.0 GPa), the twinning is strongly enhanced, while the ferroic deviation of the atomic structure is reduced. On the other hand, it has been shown that the application of pressure up to 0.5 GPa decreases the piezoelectric and electromechanical coefficients of PZN-0.09PT, and the effect is particularly strong for the shear coefficients d_{31} and k_{31}.[17] Pressure has the same effect on the shear coefficients of PMN-0.32PT.[16] This suggests that at least the large shear piezoelectric and electromechanical responses are related with the intrinsic structural complexity on the local scale rather than with the domain texture. This result is in full agreement with model calculations on single-domain and multidomain states of PNM-0.33PT,[50] demonstrating that the multidomain configuration has minor effect on both the uniaxial and shear piezoelectric responses.

IV. CONCLUSIONS

$PbZn_{1/3}Nb_{2/3}O_3$-0.1PbTiO$_3$ as representative of relaxor-based perovskite-type solid solutions at the MPB exhibits a sequence of structural changes under high pressure. First, when pressure increases from ambient to 1 GPa, the ferroelectric structural distortion is reduced, but the twinning is enhanced (the number of domains increases, and the average domain size decreases), which increases the overall strain of the average structure. This process induces a structural transformation near 1 GPa, involving a change of the preexisting multiphase (monoclinic + tetragonal) multidomain state to another, most probably, single-phase multidomain state. As a result, between 1 and 2 GPa, the ferroic structural distortion continues to be reduced, and the overall strain also decreases. Near 2 GPa, the system reaches a cubic relaxor state, in which the polar order exists only on the mesoscopic scale as polar nanoregions. The polar nanoregions persist up to 4 GPa, whereas uncoupled polar displacements of B-site cations are abundant even at 18.1 GPa. At 5.9 GPa, PZN-0.1PT undergoes a reversible pressure-induced phase transition from a cubic to an antiferrodistortive phase comprising long-range ordered antiphase octahedral tilts. Such a phase transition is typical of Pb-based perovskite-type relaxors. The contribution of order-disorder structural phenomena involved in this phase transition of PZN-0.1PT is considerable due to the persistence of uncoupled B-site-cation off-centered shifts, which in turn is a result of the complex chemistry on the B site and the associated local electric fields. At 11 GPa, the average structure reaches a saturation in the pressure-induced ferroic distortion. Up to 18.1 GPa, no further change in the tilt pattern was detected even on the local scale. The predominant polar atomic arrangements recover on decompression, but the correlation length of ferroic distortion in the final state is shorter than in the initial state. Low levels of Ru doping on the B site [Ru/(Zn + Nb + Ti) ~ 0.002] do not influence the reversible phase transition near 5.9 GPa, although the same level of doping affects the temperature-driven structural transformations at ambient pressure. The comparison between the pressure dependence of the structure and properties up to 1 GPa suggests that the remarkable piezoelectric and electromechanical responses in PZN-xPT result from intrinsic ferroic structural inhomogeneities on the mesoscopic scale rather than from the complex multidomain texture.

---

*naemi.waeselmann@uni-hamburg.de

†boriana.mihailova@uni-hamburg.de

[1] A. A. Bokov and Z. G. Ye, J. Mater. Sci. **41**, 31 (2006).

[2] M. L. Mulvihill, S. E. Park, G. Risch, Z. Li, K. Uchino, and T. R. Shrout, Jpn. J. Appl. Phys. **35**, 3984 (1996).

[3] S. E. Park and T. R. Shrout, J. Appl. Phys. **82**, 1804 (1997).

[4] D. La-Orauttapong, B. Noheda, Z. G. Ye, P. M. Gehring, J. Toulouse, D. E. Cox, and G. Shirane, Phys. Rev. B **65**, 144101 (2002).

[5] B. Noheda, D. E. Cox, G. Shirane, S. E. Park, L. E. Cross, and Z. Zhong, Phys. Rev. Lett. **86**, 3891 (2001).

[6] Y. Uesu, M. Matsuda, Y. Yamada, K. Fujishiro, D. E. Cox, B. Noheda, and G. Shirane, J. Phys. Soc. Jpn. **71**, 960 (2002).

[7]T. Scholz, B. Mihailova, G. A. Schneider, N. Pagels, J. Heck, T. Malcherek, R. P. Fernandes, V. Marinova, M. Gospodinov, and U. Bismayer, J. Appl. Phys. **106**, 074108 (2009).

[8]D. La-Orauttapong, J. Toulouse, J. L. Robertson, and Z. G. Ye, Phys. Rev. B **64**, 212101 (2001).

[9]O. Svitelskiy, D. La-Orauttapong, J. Toulouse, W. Chen, and Z. G. Ye, Phys. Rev. B **72**, 172106 (2005).

[10]E. Dul'kin, M. Roth, P. E. Janolin, and B. Dkhil, Phys. Rev. B **73**, 012102 (2006).

[11]J. H. Ko, D. H. Kim, and S. Kojima, Phys. Rev. B **77**, 104110 (2008).

[12]N. Waeselmann, B. Mihailova, B. J. Maier, C. Paulmann, M. Gospodinov, V. Marinova, and U. Bismayer, Phys. Rev. B **83**, 214104 (2011).

[13]G. Xu, Z. Zhong, H. Hiraka, and G. Shirane, Phys. Rev. B **70**, 174109 (2004).

[14]G. A. Samara, E. L. Venturini, and V. H. Schmidt, Appl. Phys. Lett. **76**, 1327 (2000).

[15]A. A. Bokov, A. Hilczer, M. Szafrański, and Z. G. Ye, Phys. Rev. B **76**, 184116 (2007).

[16]N. Yasuda, K. Fujita, H. Ohwa, M. Matushita, Y. Yamashita, M. Iwata, and Y. Ishibashi, Jpn. J. Appl. Phys. **45**, 7413(2006).

[17]N. Yasuda, Y. Itoh, H. Ohwa, M. Matushita, Y. Yamashita, M. Iwata, and Y. Ishibashi, J. Korean, Phys. Soc. **46**, 124 (2005).

[18]M. Ahart, R. E. Cohen, V. Struzhkin, E. Gregoryanz, D. Rytz, S. A. Prosandeev, H. K. Mao, and R. J. Hemley, Phys. Rev. B **71**, 144102 (2005).

[19]B. Chaabane, J. Kreisel, P. Bouvier, G. Lucazeau, and B. Dkhil, Phys. Rev. B **70**, 134114 (2004).

[20]B. Chaabane, J. Kreisel,B. Dkhil, P. Bouvier, and M. Mezouar, Phys. Rev. Lett. **90**, 257601 (2003).

[21]J. Kreisel, B. Dkhil, P. Bouvier, and J. M. Kiat, Phys. Rev. B **65**, 172101 (2002).

[22]P. E. Janolin, B. Dkhil, P. Bouvier, J. Kreisel, and P. A. Thomas, Phys. Rev. B **73**, 094128 (2006).

[23]B. Mihailova, R. J. Angel, A. M. Welsch, J. Zhao, J. Engel, C. Paulmann, M. Gospodinov, H. Ahsbahs, R. Stosch, B. Guttler, and U. Bismayer, Phys. Rev. Lett. **101**, 017602 (2008).

[24]B. J. Maier, A. M. Welsch, R. J. Angel, B. Mihailova, J. Zhao, J. M. Engel, L. A. Schmitt, C. Paulmann, M. Gospodinov, A. Friedrich, and U. Bismayer, Phys. Rev. B **81**, 174116 (2010).

[25]B. J. Maier, N. Waeselmann, B. Mihailova, R. J. Angel, C. Ederer, C. Paulmann, M. Gospodinov, A. Friedrich, and U. Bismayer, Phys. Rev. B **84**, 174104 (2011).

[26]R. J. Angel, M. Bujak, J. Zhao, G. D. Gatta, and S. D. Jacobsen, J. Appl. Cryst. **40**, 26 (2007).

[27]R. Boehler, Rev. Sci. Instrum. **77**, 115103 (2006).

[28]R. Miletich, D. R. Allan, and W. F. Kuhs, *High-Pressure Single-Crystal Techniques in High-Pressure and High-Temperature Crystal Chemistry, Reviews in Mineralogy and Geochemistry*, Vol. 41, edited by R. M. Hazen and R. T. Downs (Mineralogical Society of America, Washington, DC, 2000), pp. 445.

[29]R. G. Munro, G. J. Piermarini, S. Block, and W. B. Holzapfel, J. Appl. Phys. **57**, 165 (1985).

[30]R. J. Angel and L. W. Finger, J. Appl. Cryst. **44**, 247 (2011).

[31]R. J. Angel, D. R. Allan, R. Miletich, and W. L. Finger, J. Appl. Cryst. **30**, 461 (1997).

[32]Xu G, J. Phys. Soc. Jpn. **79**, 011011 (2010).

[33]S. Gorfman and P. A. Thomas, J. Appl. Cryst. **43**, 1409 (2010).

[34]M. Paściak, M. Wołcyrz, and A. Pietraszko, Phys. Rev. B **76**, 014117 (2007).

[35]T. R. Welberry and D. J. Goossens, J. Appl. Cryst. **41**, 606 (2008).

[36]B. J. Maier, R. J. Angel, W. G. Marshall, B. Mihailova, C. Paulmann, J. E. Engel, M. Gospodinov, A. M. Welsch, D. Petrova, and U. Bismayer, Acta Cryst. B **66**, 280 (2010).

[37]B. J. Maier, R. J. Angel, B. Mihailova, W. G. Marshall, M. Gospodinov, and U. Bismayer, J. Phys. Condens. Matter **23**, 035902 (2011).

[38]B. J. Maier, A.-M. Welsch, B. Mihailova, R. J. Angel, J. Zhao, C. Paulmann, J. M. Engel, W. G. Marshall, M. Gospodinov, D. Petrova, and U. Bismayer, Phys. Rev. B **83**, 134106 (2011).

[39]A. M. Glazer, Arcta Cryst. B **28**, 3384 (1972).

[40]B. Mihailova, R. J. Angel, B. J. Maier, A. M. Welsch, J. Zhao, M. Gospodinov, and U. Bismayer, IEEE Trans. Ultrason. Ferroelectr. Freq. Control **58**, 1905 (2011).

[41]J. Toulouse, F. Jiang, O. Svitelskiy, W. Chen, and Z. G. Ye, Phys. Rev. B **72**, 184106 (2005).

[42]A. M. Welsch, B. Maier, B. Mihailova, R. Angel, J. Zhao, C. Paulmann, J. Engel, M. Gospodinov, V. Marinova, and U. Bismayer, Z. Kristallogr. **226**, 126 (2011).

[43]A. Slodczyk, P. Daniel, and A. Kania, Phys. Rev. B **77**, 184114 (2008).

[44]M. I. Aroyo, A. Kirov, C. Capillas, J. M. Perez-Mato, and H. Wondratschek, Acta Cryst. A **62**, 115 (2006).

[45]A. Sani, B. Noheda, I. A. Kornev, L. Bellaiche, P. Bouvier, and J. Kreisel, Phys. Rev. B **69**, 020105 (2004).

[46]E. Husson, Key Eng. Mater. **155-156**, 1 (1998).

[47]B. Mihailova, U. Bismayer, B. Guttler, M. Gospodinov, and L. Konstantinov, J. Phys. Condens. Matter **14**, 1091 (2002).

[48]B. Mihailova, B. Maier, C. Paulmann, T. Malcherek, J. Ihringer, M. Gospodinov, R. Stosch, B. Guttler, and U. Bismayer, Phys. Rev. B **77**, 174106 (2008).

[49]A. M. Glazer, in *Proceedings of the European Meeting on Ferroelectricity (Abstract)*, Bordeaux, France (2011).

[50]D. Damjanovic, M. Budimir, M. Davis, and N. Setter, Appl. Phys. Lett. **83**, 527 (2003).